Electron microscopy study of direct laser deposited IN718

Ding, Rengen; Huang, ZW; Li, Hangyue; Mitchell, I.; Baxter, G.; Bowen, P.

DOI:
10.1016/j.matchar.2015.06.017

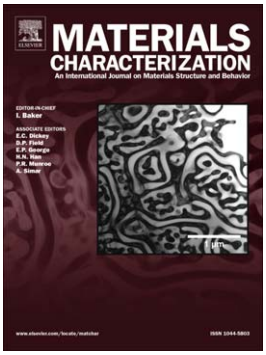

Electron microscopy study of direct laser deposited IN718

R. Ding, Z.W. Huang, H.Y. Li, I. Mitchell, G. Baxter, P. Bowen

PII: S1044-5803(15)00223-5
DOI: doi: 10.1016/j.matchar.2015.06.017
Reference: MTL 7937

To appear in: *Materials Characterization*

Received date: 22 March 2015
Revised date: 17 June 2015
Accepted date: 18 June 2015

Please cite this article as: Ding R, Huang ZW, Li HY, Mitchell I, Baxter G, Bowen P, Electron microscopy study of direct laser deposited IN718, *Materials Characterization* (2015), doi: 10.1016/j.matchar.2015.06.017

Electron microscopy study of direct laser deposited IN718

R. Ding[1*], Z.W. Huang[1], H.Y. Li[1], I. Mitchell[2], G. Baxter[2], and P. Bowen[1]

1. School of Metallurgy and Materials, The University of Birmingham, Edgbaston, Birmingham B15 2TT, United Kingdom

2. Rolls-Royce plc. Derby DE24 8BJ, United Kingdom

* - corresponding author, e-mail: r.ding@bham.ac.uk; Tel. 0044-121-4145211; Fax: 0044 -121-4145232

Abstract

The microstructure of Direct Laser Deposited (DLD) IN718 has been investigated in detail using scanning electron microscopy (SEM) and transmission electron microscopy (TEM). The results confirm that the dendrite core microstructure can be linked to the cooling rate experienced during the deposition. A ~ 100 μm wide δ partially dissolved region in the IN718 substrate was observed close to the substrate/deposit boundary. In the deposited IN718, γ/Laves eutectic constituent is the predominant minor microconstituent. Irregular and regular (small) (Nb,Ti)C carbides and a mixture of the carbides and Laves were observed. Most M_3B_2 borides were nucleated around a (Nb,Ti)C carbide. Needles of δ phase precipitated from the Laves phase were also observed. A complex constituent (of Laves, δ, α-Cr, γ′′, and γ matrix) is reported in IN718 for the first time. The formation of α-Cr particles could be related to Cr rejection during the formation and growth of Cr-depleted δ phase.

Key words: IN718, Laser deposition, Microstructure, TEM

1. Introduction

Direct laser deposition (DLD) using blown powder is a near net-shape manufacturing method which feeds a metal powder through a nozzle into the focal point of a laser beam. The laser melts the powder producing a deposit onto a pre-existing substrate. A structural shape is formed via the powder nozzle and the laser beam moving relative to the substrate surface in a raster pattern. A part is built up layer by layer until the required shape is obtained. Meanwhile, a fine microstructure can be obtained due to the non-equilibrium rapid solidification process, which would bring about superior mechanical properties. The DLD process can be used to manufacture components with complex internal geometries that would be difficult to machine or cast, and repair worn parts, such as turbine blades and disks. The high replacement cost of

gas turbine engine components makes DLD a promising application in the repair of worn components [1].

IN718 is a niobium-modified age-hardenable nickel-base superalloy which has precipitating γ′′ (Ni_3Nb) and γ′ ($Ni_3(Al,Ti)$) phases in the γ matrix. The alloy is one of the most common Ni-base superalloys and is used for numerous applications in the aerospace and nuclear industries because of its good strength, excellent resistance to oxidation and favourable weldability. Extensive research on the microstructure of welded IN718 has been performed [2-9], mostly concerned with gas tungsten arc (GTA) and electron beam (EB) welds [2-7]. In contrast, very little published work is available on DLD IN718 [9-11].

DLD processing is dramatically different from the other welding processes (e.g. GTA and EB welding) and casting as it produces a small molten pool, resulting in a fast cooling rate and the formation of a non-equilibrium structure. Thus, the microstructure of DLD IN718 is different from other welded forms of IN718, especially with regard to secondary phases and their distributions which, in turn, would affect the mechanical behaviour. Although some recent research on the microstructure of laser deposited IN718 has been performed [1, 10, 11] and some secondary phases (e.g. carbide, Laves phase and needle-like δ phase) have been reported [10-14], there is a lack of detailed investigation, particularly at the TEM level. The current paper uses TEM to identify secondary phases of DLD IN718 to aid in understanding the mechanical behaviour of DLD IN718. A complex constituent (of Laves, δ, α-Cr, γ′′, and γ matrix) is reported here in IN718 which, to the authors' knowledge is the first time this constituent has been reported.

2. Experimental procedure

Commercially available Plasma Rotating Electrode Processed (PREP) IN718 powder with a mesh size between +325 and −100 was used in this study. The powder has a nominal composition (wt.%): 53Ni, 19Fe, 18Cr, 5.2Nb, 3.0Mo, 1.0Ti, 0.6Al, 0.05C and 0.006B. DLD was undertaken on a wrought IN 718 substrate with dimensions of 13mm × 50mm × 50 mm in a YAG laser deposition system. A low power of 350 W (fast cooling rate, referred as Sample A) and a high power of 550 W (low cooling rate, Sample B) were used for the deposits to produce near fully dense deposits. Pure argon was used as a shield gas to prevent the molten pool from oxidation and contamination. The as-deposited samples were aged at the standard 732°C/4 hrs + 649°C/ 4 hrs.

Samples for optical and SEM were prepared following a standard metallographic procedure. The polished surface was etched in a reagent of 10 ml HNO_3, 20 ml HCl, 25 ml distilled water and 10 ml hydrogen peroxide (H_2O_2). The SEM examination was performed using a FEI Quanta 3D. The size of dendrite cores was determined using ImageJ software from SEM observations of over 500 cores. Specimens for TEM were prepared by mechanically grinding 3 mm diameter discs to ~ 150 μm and then twin-jet electropolishing them in a solution of 10% perchloric acid, 30% butanol and 60% methanol at 243 K and 25V. TEM observation was carried out on a FEI Tecnai F20 microscope operating at 200 kV and equipped with an Oxford Instruments silicon drift detector (SDD) for energy-dispersive X-ray spectrometry (EDS). The K_a lines were used for Ni, Fe, Cr, Ti, Si and Al, while the L_a lines were used for Nb and Mo. Raw data were reduced to atomic percentages using a ZAF algorithm. The size of second phases was determined using ImageJ software from TEM observations of over 500 particles.

3. Results and Analysis

3.1 Microstructure of the substrate

The substrate shows a typical microstructure for standard heat-treated IN718: an average grain size of 6 μm with a large number of particles at grain boundaries and interior grains (Figs. 1a and 1b). The particle size ranges from ~ 200 nm to 2 μm. EDS analysis shows that they are a Nb-rich phase (Fig. 1c and Table 1). Analysis of diffraction patterns in Figs. 1d-f confirms that the Nb-rich particles are orthorhombic Ni_3Nb-type δ phase with lattice parameters a = 0.51 nm, b = 0.43 nm and c = 0.46 nm. In the pattern, streaks parallel to the (010) reflection are observed, these are attributed to the presence of stacking faults in the δ phase (Fig. 2). Fig. 3a shows the [001] diffraction pattern of the matrix and visible extra reflections, which indicate the presence of a large amount of γ′ (Fig. 3b) and γ′′ (Fig. 3c) phases. The average γ′ particle size is 23 nm and the average γ′′ particle size is 42 nm (long axis) by 12 nm (short axis).

3.2 Microstructure of the deposit

The images in Fig. 4 are low magnification optical micrographs of the laser-fabricated blocks showing the deposited layers. A montage SEM image of the substrate/deposit is shown in Fig. 5, which exhibits elongated coarse grains in the deposit. Such elongated coarse grains crossing several deposit layers can also be observed clearly in optical micrographs (Fig. 4a).

Their existence is a direct consequence of epitaxial growth and preferred growth along the <001> direction. A high thermal gradient at the liquid/solid interface and a low solidification velocity are the necessary conditions for epitaxial growth, and these are usually achieved in laser deposit process. However, a band of fine grains was found in the deposit close to the substrate/deposit boundary. This could be associated with higher cooling rates close to the substrate.

Closer examination around the substrate/deposit boundary revealed that there is an approximately 100 μm wide zone where the δ phase had partially dissolved close to the boundary, in the substrate (Fig. 5). This means that the δ phase particles are dissolved during deposition (δ solvus temperature = 996~1015°C [15]). In other words, during deposition, the temperature at a region 100 μm away from the boundary is above the (996~1015°C). δ dissolution would produce a higher Nb content in the matrix, which might promote the formation of a higher density of γ″ and γ′ precipitation in this region during subsequent deposition and/ ageing. It is thus expected the strength will be higher in this region [16].

Fig. 6 shows cross-section (i.e. parallel to the deposit layer) SEM images from the deposited materials in samples A and B. Sample A has fine dendrite cores (5.2±1.1 μm) compared with sample B (6.5±1.8 μm). Sample A was deposited using a faster cooling rate during solidification, resulting in a finer dendrite structure, thus improving the strength of the deposit [16]. In contrast to the dark dendrite core, small white constituents in globular and irregular shapes have formed along the interdendritic regions (Fig. 6). The interdendritic region was indentified by EDS to have a relatively high Nb content compared with the matrix, which is consistent with previous publications [1, 9, 10]. Compositions and structures of secondary phases in the deposit have been determined using TEM as discussed in the following subsections.

3.2.1 γ′ and γ′′ phases

The main precipitates in the laser deposited IN 718 are γ′ and γ′′, as shown in Fig. 7. The average size is 13.8 nm for γ′ and 13.4 nm (long axis) and 3.8 nm (short axis) for γ′′ after heat treatment. They are smaller compared with precipitates in the substrate because there is lower Nb content in the dendrite core regions due to interdendritic microsegregation which gives rise to a low rate of nucleation and growth of γ′′ during the following ageing treatment.

3.2.2 γ/Laves eutectic

In TEM examination, a large number of precipitates were observed in interdendritic regions and at grain boundaries in the deposit samples. Figure 8 shows that they distribute along grain boundaries in some cases as discontinuous (Fig. 8a) and in others as continuous (Fig. 8b) phases. Fig. 8b shows that there may be two types of precipitate, and that they are mixed and distributed along the grain boundaries. A higher magnification image is shown in Fig. 9a. EDS analysis indicates that the dark phase is Nb-rich and the composition is close to $(Ni,Cr,Fe)_2(Nb,Mo,Ti)$ (at.%) (Fig. 9b and Table 1). Diffraction patterns in Fig. 9c-e confirm that the dark phase is hexagonal $MgZn_2$-type (C14) Laves phase with lattice parameters a = 0.47 nm and c = 0.77 nm. EDS examination revealed that the grey phase has higher Cr and Fe compared with the matrix (Fig. 9f). Analysis of the diffraction pattern in Fig. 9f confirms that the grey phases are γ. Such a mixture is, thus, designated as γ/Laves eutectic. This eutectic has been well documented in as-cast and welded IN718 [4, 17, 18]. Laves phase has been demonstrated to be the source of crack initiation in for DLD IN718 [16]. When laves phase is continuously distributed in the interdendritic regions and/or along grain boundaries, the sample shows low ductility and fatigue life [16]. Fast cooling rate tends to a propensity of a continuous distribution of laves phase [16].

3.2.3 Carbides

Nb-rich carbides were usually observed, commonly appearing irregular in shape (Fig. 10a and b), which suggests that the carbides formed during solidification. This is consistent with the fact that the carbide has a high melting point (~3600°C for NbC) [19], much higher than that of IN718 (1364°C) [20]. Diffraction patterns in Fig. 10e-g confirm that these Nb-rich carbides have a cubic NaCl-type structure with lattice parameter a = 0.44 nm. Small and regular MC carbides were also observed (Fig. 10c), which suggests that this type of carbide precipitates from the solid state during cooling. This is associated with the fact that the solubility of C in Ni is low and dramatically decreases with temperature [21]. An irregular constituent consisting of NbC and Laves was found occasionally, as shown in Fig. 11.

3.2.4 Complex constituent

A constituent consisting of many small particles (which might be different phases) was commonly observed, as shown in the centre of Fig. 10a and in Fig. 12. EDS mapping (Fig. 12) and spot EDS (Fig. 13a) show that some of the particles are Cr-rich while the others are (Nb,Fe,Mo)-rich and (Nb,Ni)-rich. Spot EDS shows that the Cr-rich particles contain small

amounts of Mo, Fe and Ni (Fig. 13 a and Table 1). Diffraction patterns in Fig. 13 confirm that the Cr-rich particles are *bcc* α-Cr with lattice parameter a = 0.29 nm. To the authors' knowledge, the α-Cr particle has not been reported in as-cast and welded IN718 in the open literature. The EDS analysis and diffraction patterns (Fig. 13) indicate that the other particles are Laves phase, irregular shaped δ phase, needle-like γ′′ and the matrix (accurately speaking, γ+γ′+γ′′). Such needle-like γ′′ particles are also distributed in the matrix (Fig. 12a, b and h). They have a composition similar to that of the δ phase (Figs. 12h and 13a and Table 1) but have a tetragonal structure with a = 0.36 nm and c = 0.74 nm confirmed via diffraction (Fig. 13g). The diffraction pattern (Fig. 13g) also shows $(112)_{\gamma''}$ parallel to $(111)_{\gamma}$. The γ′′ particle has a regular (needle-like) shape and the orientation relationship with the γ phase suggests that the γ′′ particle precipitates from the γ phase in the solid state. Examination of an as-deposited sample shows there are no such needle-like γ′′ particles in the complex constituent, which indicates that such needle-like γ′′ formed during the ageing heat treatment after the DLD process.

Fig. 12 also shows that the distribution of α-Cr particles is associated with the δ phase. This could be related to the fact that the δ phase is Cr-depleted, thus Cr is rejected from the δ phase during its formation and growth. The nucleation and growth of α-Cr on the surface of an advancing δ phase have been demonstrated in IN718 aged for a long time [22-26] and in a shorter time under stress [27].

3.2.5 Needles in the Laves phase

It is interesting that needle-like particles in a Nb-rich phase were occasionally observed (Fig. 14a). EDS linescans (Figs. 14b-g) across a needle-like particle show that the needle-like particle has an equivalent Nb content (~27 at.%) to the Nb-rich phase but higher Ni and lower Cr, Fe and Mo. Quantitative EDS analysis shows that the composition of the needle-like particles is closest to $(Ni,Cr,Fe)_3(Nb,Ti)$ while the Nb-rich phase is close to $(Ni,Cr,Fe)_2(Nb,Mo,Ti)$ (see Table 1), indicating that they could be the δ phase and Laves phase, respectively. Composite diffraction patterns from the needle-like phase and Nb-rich phase in Fig. 14h, further confirm that the needle-like particle is the δ phase and that the Nb-rich phase is Laves phase, and also indicate that there is an orientation relationship between the δ and the Laves:

$$(010)_{\delta}//(\bar{1}010)_{\text{Laves}}$$

$$[100]_{\delta}// [\bar{1}2\bar{1}6]_{\text{Laves}}$$

The analysis of the diffraction pattern also indicates that the preferred growth direction of the δ phase is parallel to the [001] direction. Fig. 14i is a dark field image of the δ phases obtained using the (001) reflection. The regular needle-like shape and the orientation relationship with the Laves phase, suggests that the δ phase precipitates in the Laves phase in the solid state. The δ phase precipitated from the Laves phase was also found in the as-deposited sample but there were fewer precipitates than in the aged sample. This suggests that subsequent ageing promotes the precipitation of δ phase from the Laves phase. Since the δ phase is Mo, Fe and Cr-depleted but Ni-rich compared with the Laves phase (Fig. 14), during the growth of the δ phase, Mo, Fe and Cr will be rejected into the Laves and more Ni is needed, thus bringing about higher Mo, Fe and Cr and lower Ni at the Laves/δ interface compared with the Laves phase (Fig. 14). Note that the dashed line in each element profile presents the average content of the element in the Laves phase. The presence of δ phases is not unusual in cast microstructures. In the tungsten-gas-shaped metal deposit Clark et al. [28] observed needle-like phases and assumed the needles to be δ phase. Wlodek and Field also reported that δ phase precipitated in the large Laves phase particles in the freckled areas of large IN 718 structural investment castings [29].

Extensive research has been carried out on the phase transformation under both continuous cooling and isothermal conditions [30-32], that indicates the precipitation temperature of δ phase is lower than that of Laves phase. Fig. 15a shows the continuous-cooling-transformation (CCT) curves of IN 718 from 1180°C [30], which indicates that the δ phase will form when the cooling rate is lower than 9°C/sec. The δ phase cannot form in as-welded or as-cast metal, which may be attributed to the fast cooling rates during welding and casting. Reddy et al. [33] found that solution treatment of laser welded IN 718 at 980°C resulted in partial dissolution of Laves phase and that the relative ease with which dissolution occurred was a function of its size, morphology, and Nb concentration. They also observed the precipitation of δ phase around the partially dissolved Laves particles. Solution treatment at 1080°C was found to lead to complete dissolution of Laves phase [33]. This has also been demonstrated in the post weld heat-treated IN 718 electron beam welds [34]. Laves phase can, therefore, be dissolved in the range of 980-1080°C, which is higher than the temperature range of its precipitation (860-995°C) [35]. During laser deposition, the prolonged and potentially cumulative exposure to high temperatures during cooling and repeated thermal excursions from adjacent deposition passes, together with the fact that δ phase has a similar

Nb content to Laves phase (Fig. 14 and Table 1), allows the precipitation of δ phase from Laves phase to occur.

3.2.6 Boride

A boride phase was also observed (Fig. 16). Irregular-shaped boride particles (Fig. 16a) could form during solidification while small boride particles (Fig. 16a) precipitated after solidification. Most of the borides nucleated around (Nb,Ti)C carbides, as shown in Fig. 16b, which is consistent with some investigations on as-cast [29] and welded IN 718 [4]. Fig.16c exhibits a typical EDS spectrum from the boride, showing that the boride is (Mo, Nb)-rich (Table 1). Diffraction analysis indicates that the boride is tetragonal M_3B_2 with a = 0.58 nm and c = 0.32nm. This type of boride is often observed in Ni-base superalloys [4, 29, 36, 37].

After the detailed examination of the deposits, the results can be summarized as follows: 1) Irregular and regular (small) (Nb,Ti)C carbides and a mixture of the carbides and Laves phase were observed. The irregular carbides and the mixture are considered to form during solidification while the regular carbide precipitates form from the matrix in the solid state. 2) Most of the M_3B_2 borides were nucleated around a (Nb,Ti)C carbide. 3) γ/Laves phase eutectic, which is the predominant minor constituent in the deposit, was commonly found along grain boundaries. 4) The complex constituent consisting of Laves phase, δ phase, α-Cr, γ′′ and matrix (accurately speaking, γ+γ′+γ′′) was easily found and is reported in welded IN718 for the first time. The formation of α-Cr is considered to be associated with the formation of Cr-depleted δ phase. 5) Needles of δ phase precipitated from the Laves phase were also observed. In the following section the formation of these constituents by solidification path of IN718 is considered.

4. Discussion

As mentioned in the introduction, the aim of this study is to investigate the secondary phases formed in the deposits. The secondary phases observed were not altered by the change in cooling rate resulting from the different deposition parameters. Thus, this discussion focuses on the types of secondary phases observed, some of which were only observed in DLD IN718. The solidification sequence of IN718 has been established previously [14, 18, 20]. The solidification path begins with the formation of γ dendrites. Solute elements with a partition coefficient, $k < 1$ would be rejected into the interdendritic liquid (e.g. Nb, Ti, C, B). When the

contents of these solute elements in the interdendritic liquid exceed their solubility limit, secondary solidification constituents start to form. In Ni-base superalloys there are several possible secondary solidification constituents including carbides, borides and a number of other intermetallic constituents. For IN 718 alloy, the strong carbide forming elements Nb and Ti continually enrich in the interdendritic liquid, which could eventually result in formation of MC carbides. This is most likely to occur via a non-invariant eutectic type reaction of L→ γ + NbC at 1250°C [17, 20]. In this study, the distribution of irregular NbC carbides as shown in Fig. 10b appears to be similar to those found in a γ/NbC eutectic [20], although eutectic γ is not observed. This may be because reheating from subsequent deposition passes and ageing treatments could bring about the precipitation of γ′ and γ′′ from the original eutectic γ and make the eutectic γ undistinguishable from the matrix. The formation of the γ/NbC constituent depletes the interdendritic liquid of most of C content. However, as γ dendrite formation continues, enrichment of the remaining liquid with Nb will continue until the eutectic reaction L→ γ + Laves occurs [17, 20]. Thus large amounts of γ/Laves eutectics were observed (Fig. 8 and 9) and this constituent is considered to be the predominant minor microstructural feature in IN718 weld metal [20]. The formation of the Laves phase can deplete principal alloying elements required for hardening from the matrix and acts as a preferential site for crack initiation and propagation [13, 16, 38]. Its inherent brittle nature brings about poor tensile ductility, fracture toughness, creep and fatigue properties in IN718 [16, 39]. The Laves phase is, thus, detrimental and should be carefully controlled.

It is interesting that the γ/Laves eutectic was also observed around, or connected to, the carbides, as shown in Figs. 11 and 14a. Parimi et al. [14] also found that fine carbides were embedded in the Laves phase in direct laser fabricated IN718. This is likely to occur because when carbides form the local surrounding liquid becomes depleted in C but still enriched in Nb, thus favouring the eutectic reaction L→ γ + Laves. Knorovsky et al. [20] also mentioned that it is possible to have a four phase equilibrium (L→ γ + NbC + Laves). Furthermore, based on the available liquidus projection for the Ni-NbC-Ni_3Nb triangle, Radhakrishnan and Thompson [17] considered that the reaction L→ γ + NbC + Laves could take place in IN718 if Ni_3Nb is replaced by the Laves phase and if Ni is replaced by γ. They also suggested that the γ/NbC/Laves eutectic in IN 718 could have two distinct microstructural morphologies: an intimate three-phase mixture or a divorced eutectic. The microstructure shown in Fig. 11

appears to be a divorced eutectic. A similar microstructure was also reported by Vincent [4] in fusion zones of IN718 welds.

A considerable number of the complex constituent (α-Cr + δ + Laves + γ′′ + matrix) (Figs. 10 and 12) were observed in the present investigation, which has not been reported previously in as-cast and welded IN 718. Clearly, the formation of this complex constituent cannot be explained by the available solidification path of IN 718. One reasonable explanation is that this constituent initiates from γ/Laves eutectic. The CCT (Fig. 15a) and TTT (Fig. 15b) diagrams indicate that δ phase is more stable than the Laves phase. This is also supported by the present (Fig. 14) and the other authors' [13, 14, 28, 29] observations on the precipitation of the δ phase from the Laves phase. Parimi et al. [14] found the δ phase protruding from Laves phase in direct laser fabricated IN718 while Clark et al. [28] observed needle-like δ phases related to Laves phase in the tungsten-gas-shaped metal deposited IN718. Zhang et al. [13] found that post solution heat treatment leads to partial dissolution of Laves particles at a solution temperature of 954°C and the precipitation of needle-like δ phase around the Laves particles in laser deposited IN718 using filler wire. During deposition, adjacent passes could possibly heat previous layers to a high enough temperature for a considerable time [28], leading to the precipitation of the δ phase from the Laves phase. The formation of the δ phase would reject Cr and Fe to the Laves and γ phases. As Fe has a higher solubility in Ni, Fe rejected from the δ phase could dissolve in the γ phase. However, since the solubility of Cr in Ni decreases significantly with decreasing temperature, Cr rejected from the δ phase would exceed its solubility limit and then form α-Cr particles. This leads to the distribution of α-Cr particles associated with the δ phases (Fig. 12h). The formation of α-Cr on advancing δ phase has been demonstrated in IN 718 after a long term ageing treatment [22-25]. Large needle γ′′ in the complex constituent are also precipitated from the γ phase during post deposition ageing treatment.

5. Conclusions

This study has investigated the detail of microstructure in IN718 deposited by DLD using SEM and TEM techniques, focussing on identifying secondary phases in the deposit. The following main conclusions are drawn:

1) Fast cooling brings about fine dendrite cores;

2) A ~ 100 µm wide zone where δ phase had partially dissolved was observed close to the substrate/deposit boundary in the substrate.
3) (Nb,Ti)C carbide, M_3B_2 boride and γ/Laves eutectic were usually observed. The mixture of the carbides and Laves (probably designated to γ/NbC/Laves eutectic), was found. The predominant minor constituent γ/Laves eutectic tends to distribute along grain boundaries as discontinuous phases, which may degrade mechanical behaviour.
4) A complex constituent phase consisting of Laves phase, δ phase, α-Cr, γ″ and the matrix (accurately, the γ+γ′+γ″) was commonly observed. The formation of α-Cr is considered to be associated with the formation of Cr-depleted δ phase during adjacent deposition.

ACKNOWLEDGEMENTS

The authors would like to thank Rolls–Royce plc for financial support and for the provision of test pieces. The work was part-funded by the Engineering Physical Science Research Council (EPSRC) of the United Kingdom (EP/H022309/1).

References

1. P. L. Blackwell: *J. Mater. Proc. Technol.*, 2005, vol. 170, pp240-246.
2. Ch. Radhakrishna and K. Prasad Rao: *Mater. High Temp.*, 1994, vol. 12 (4), 323.
3. Ch. Radhakrishna and K. Prasad Rao: *J. Mater. Sci.*, 1997, vol. 32, P1.
4. R. Vincent: *Acta metall.*, 1985, vol. 33, p1205-16.
5. K. Sivaprasad and S. Ganesh Sundara Raman: *Metall. Trans. A*, 2008, vol. 39A, p2115.
6. R. G. Thompson and S. Genculu: *J welding*, 1983, vol. 62, p337-345.
7. G. Madhusudhana Reddy, C. V. Srinivasa Murthy, K. Srinivasa Rao and K. Prasad Rao: *Int. J. Adv. Manuf. Technol.*, 2009, vol. 43, pp 671-680
8. A. Odabasi, N. ünlu, G. Göller and M. N. Eruslu: *Metall. Trans. A*, 2010, vol. 41, P2357-2365.
9. G. D. Janaki Ram, A. Venugopal Reddy, K. Prasad Rao, G. M. Reddy and J. K. Sarin Sundar: *J. of Mater. Proc. Technol.*, 2005, vol. 167, pp73-82.
10. H. Qi, M. Azer and A. Ritter: *Met. Trans. A*, 2009, vol. 40, P2410
11. X. M. Zhao, J. Chen, X. Lin and W. D. Huang: *Mater. Sci. Eng. A*, 2008, vol. 478, pp119-124.

12. Z. M. Wang, K. Guan, M. Gao, X. Y. Li, X. F. Chen and X. Y. Zeng: *J. Alloys and Compounds*, 2012, vol. 513, pp 518-523.
13. Y. N. Zhang, X. Cao and P. Wanjara: *Int J Adv Manuf Technol.* 2013, vol. 69, pp 2569-2581.
14. L. L. Parimi, G. A. Ravi, D. Clark and M. M. Attallah: *Mater. Char.*, 2014, vol. 89, pp102-111.
15. W. D. Cao: in *Superalloys 718, 625, 706 and Various Derivatives***,** E.A. Loria, ed., TMS, Warrendate, PA, 2005, pp165-177.
16. Z.W.Huang, R.G.Ding, I.Mitchell, G.Baxter, P.Bowen. Unpublished results, 2014.
17. B. Radhakrishnan and R. G. Thompson: *Metall. Trans. A*, 1989, vol. 20, P2866.
18. J. N. DuPont, C. V. Robino, and A. R. Marder: *J. Welding*, 1989, vol. 77, pp.417s.
19. E. K.Storms: Refractory Carbides. New York: Academic Press; 1968
20. G. A. Knorovsky, M. J. Cieslak, T. J. Headley, A. D. Romig, Jr., and W.F.Hammetter: *Metall. Trans. A*, 1989, vol. 20A, pp2149.
21. J. J. Lander, H. E. Kern and A. L. Beach: *J. Appl. Phys.*, 1952, vol.23, pp1305-1309.
22. Z. N. Bi, J. X. Dong, M. C. Zhang, L. Zheng, and X. S. Xie, *Inter. J. Miner. Metall. and Mater.*, 2010, vol.17, pp312.
23. D. Srinivasan, *Mater. Sci. & Eng. A*, 2004, vol.364, pp27-34.
24. B. A. Lindsley, X. Pierron, and G. E. Maurer: in *Long term stability of high temperature materials*, G. E. Fuchs, K. A. Dannemann and T. C. Deragon, ed., TMS, Warrendale, PA 1999, pp23-133.
25. S. T. Wlodek and R. D. Field, in *Superalloys 718, 625, 706 and Various Derivatives*, E. A. Loria, ed., TMS, Warrendale, PA, 1994, pp659-670
26. J. W. Brooks and P. J. Bridges, in *Superalloys 1988*, S. Reichman, et al. ed., TMS, Warrendale, PA, 1988, pp33-42.
27. S.J. Patel and G.D. Smith, the Role of Niobium in Wrought Superalloys.
28. D. Clark, M. Bache and M. T. Whittaker: *Met. Trans. B*, 2010, vol. 41, pp1346-1353.
29. S. T. Wlodek and R. D. Field: in *Superalloys 718, 625, 706 and Various Derivatives*, E. A. Loria, ed., TMS, Warrendale, PA, 1994, P167-176.
30. C. I. Garcia, A. K. Lis, E. A. Loria, and A. J. DeArdo: in *Superalloys 1992*, S. D. Antolovich, R. W. Stusrud, R. A. MacKay, D. L. Anton, T. Khan T, R. D. Kissinger, and D. L. Klarstrom, eds., TMS, Warrendale, PA, pp. 527–36.
31. A. Lingenfelter: in *Superalloy 718-Metallurgy and Applications*, E. A. Loria, eds., 1989, TMS, Warrendale, PA, pp.673.

32. D. D. Keiser and H. L. Brown: "A Review of the Physical Metallurgy of Alloy 718", Aerojet Nuclear Company, ANCR-1292, UC-25, Idaho National Engineering Laboratory, 1976.
33. G. Madhusudhana Reddy, C. V. Srinivasa Murthy, K. Srinivasa Rao, and K. Prasad Rao: *Int. J. Adv. Manuf. Technol.*, 2009, vol. 43, pp.671-680.
34. G. D. Janaki Ram, A. Venugopal Reddy, K. Prasad Rao, G. M. Reddy, and J. K. Sarin Sundar, *J. of Mater. Proc. Technol.*, 2005, 167, pp.73-82.
35. J. F. Radavich: in *Superalloy 718-Metallurgy and Application*, 1989, E. A. Loria eds. TMS, Warrendale, PA, P229.
36. O. A. Ojo and H. R. Zhang, *Met. Trans. A*, 2008, vol. 39, pp.2799-2803.
37. J. Garofano, H.L. Marcus and M. Aindow, *Mater. Char.*, 2010, vol.61, pp929-936.
38. X. Cao, B. Rivaux, M. Jahazi, J. Cuddy and A. Birur, *J Mater. Sci.*, 2009, vol. 44, pp4557-4571.
39. S. Biswa, G. M. Reddy, T. Mohandas, C. V. S. Murthy, *J Mater. Sci.*, 2004, vol. 39, pp6813-6815.

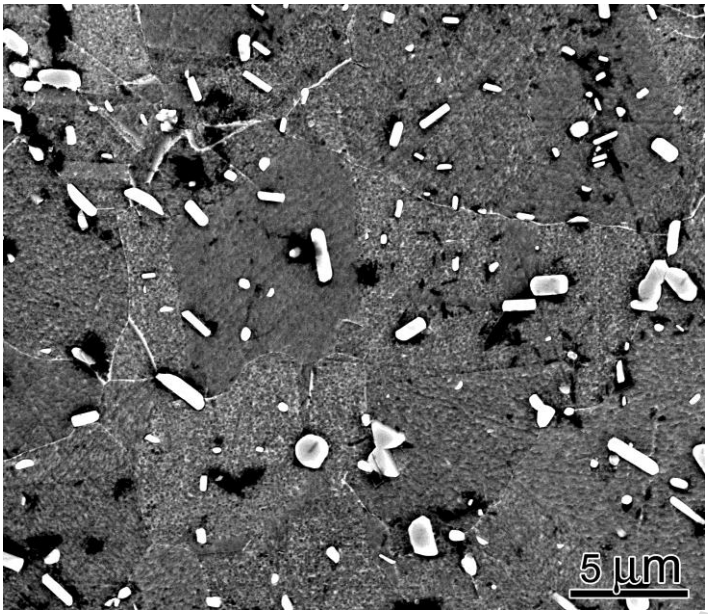

(a)

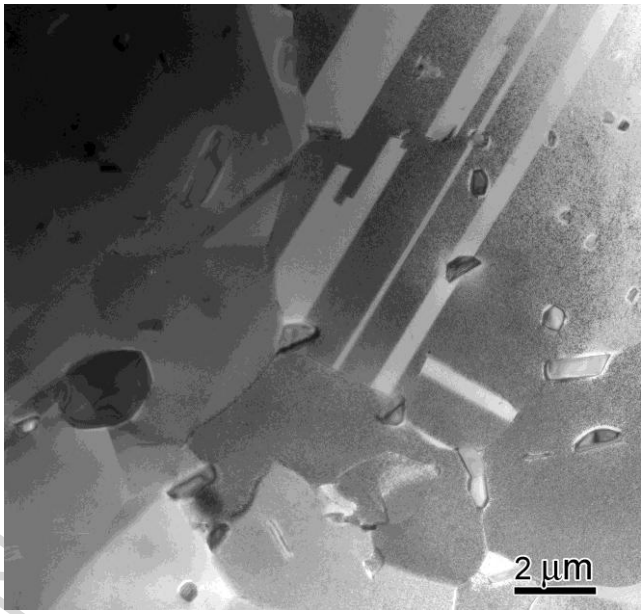

(b)

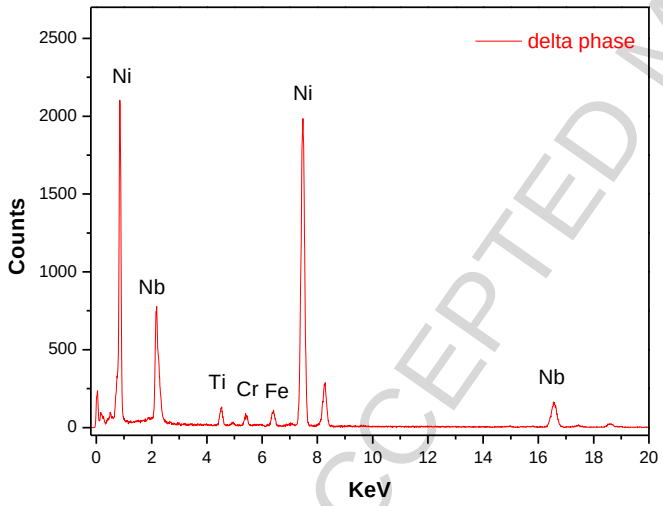

(c)

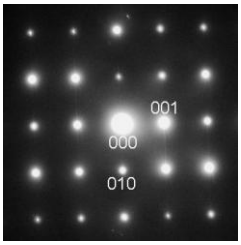

(d)

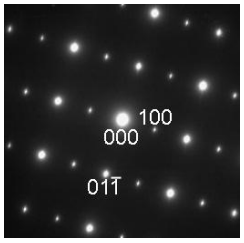

(e)

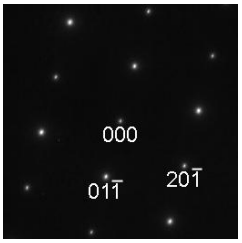

(f)

Figure 1

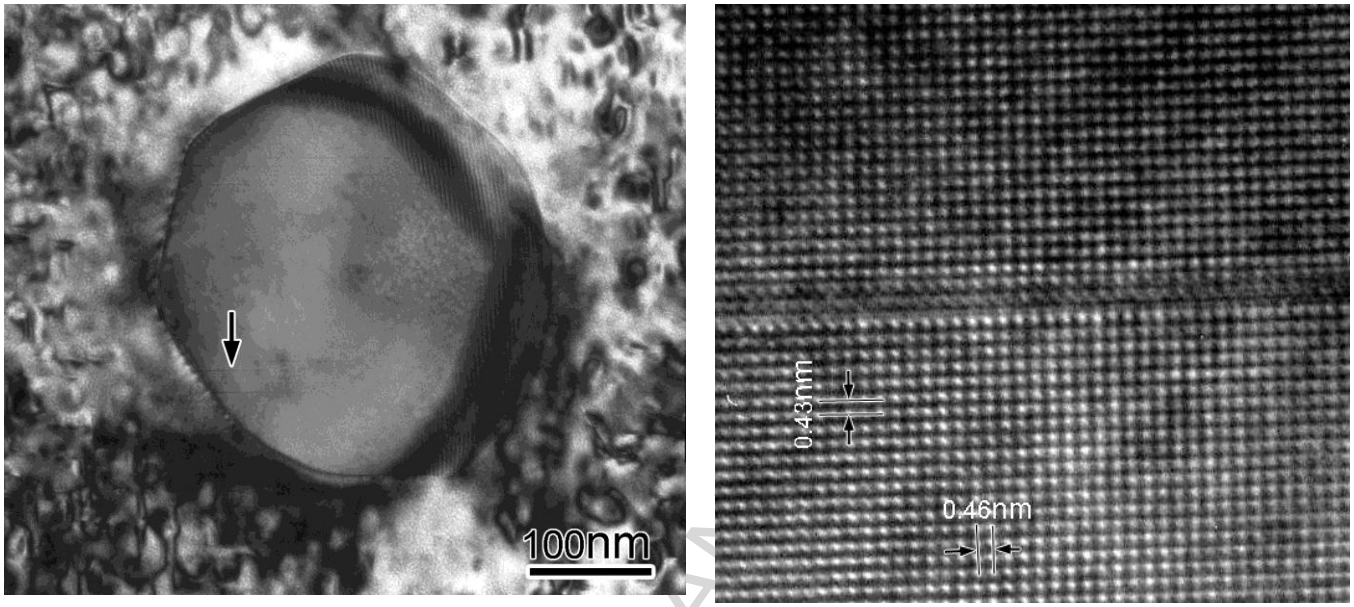

(a) (b)

Figure 2

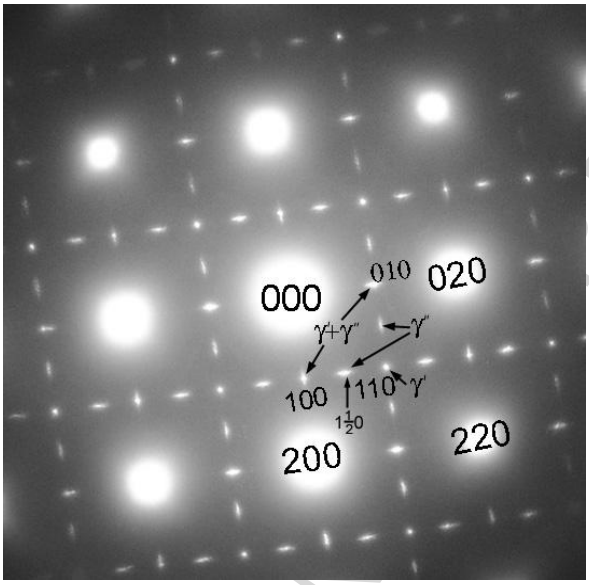

(a)

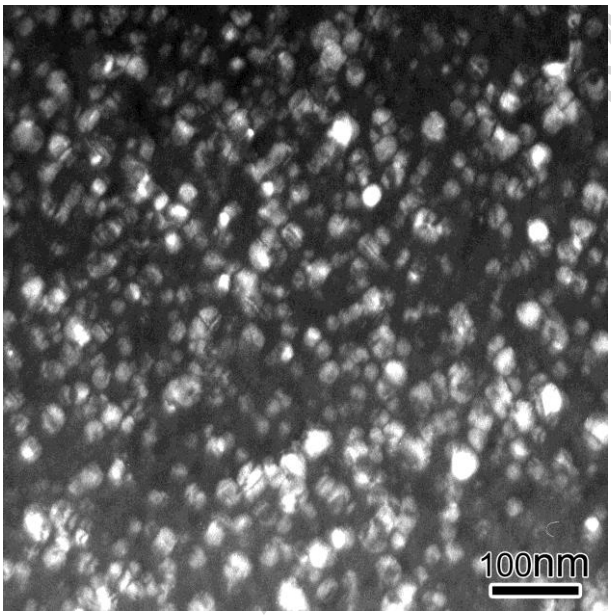

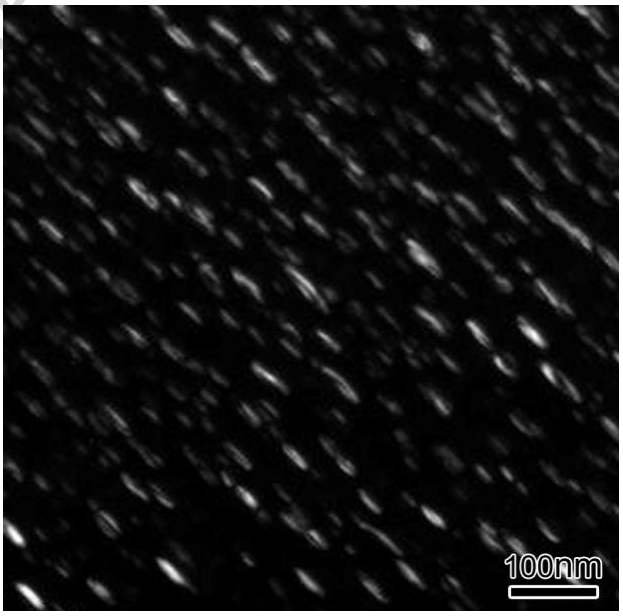

(b) (c)

Figure 3

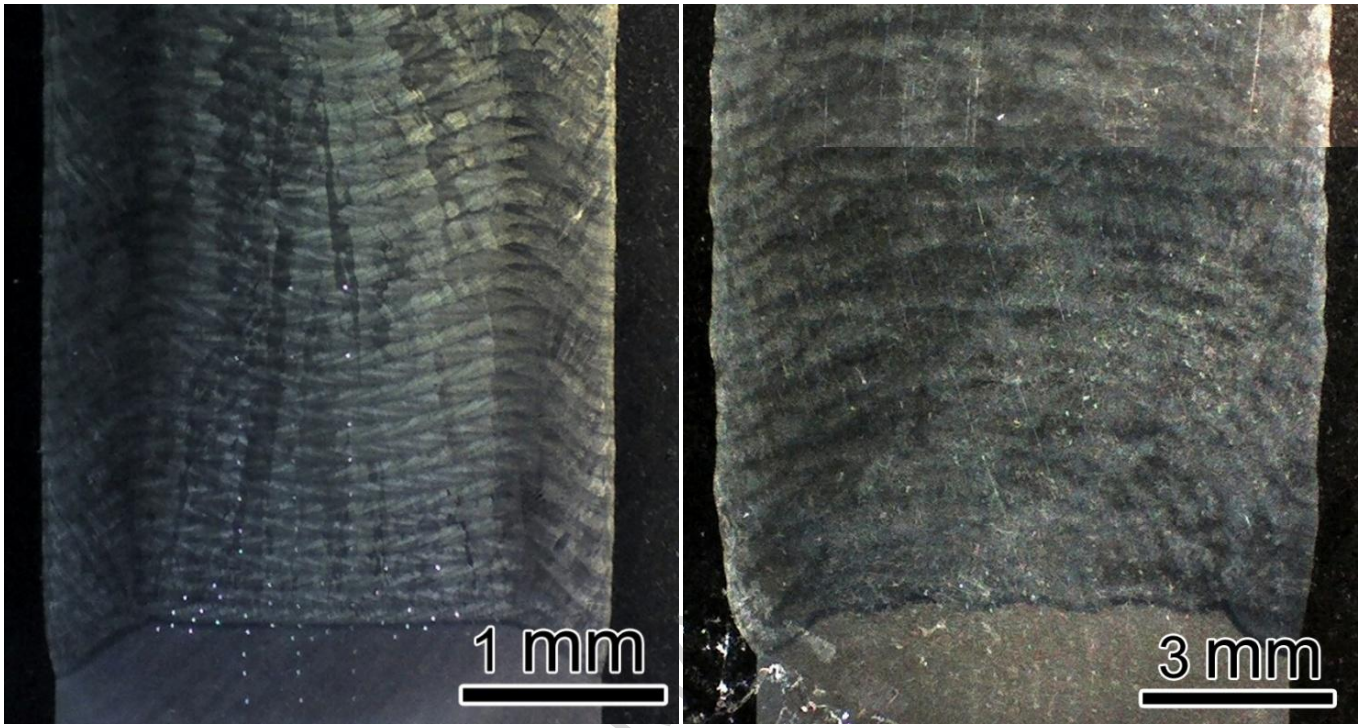

(a) (b)

Figure 4

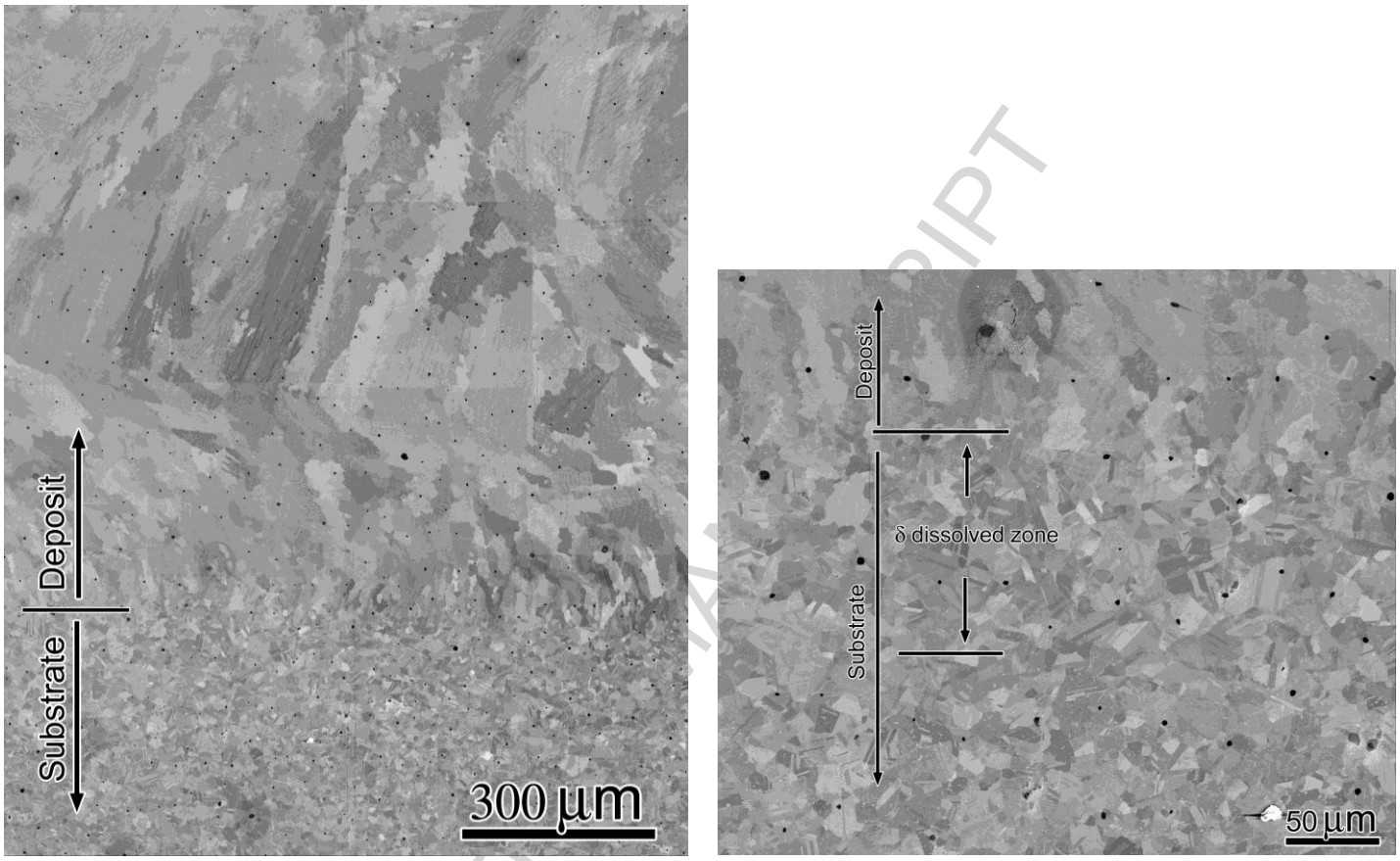

(a) (b)

Figure 5

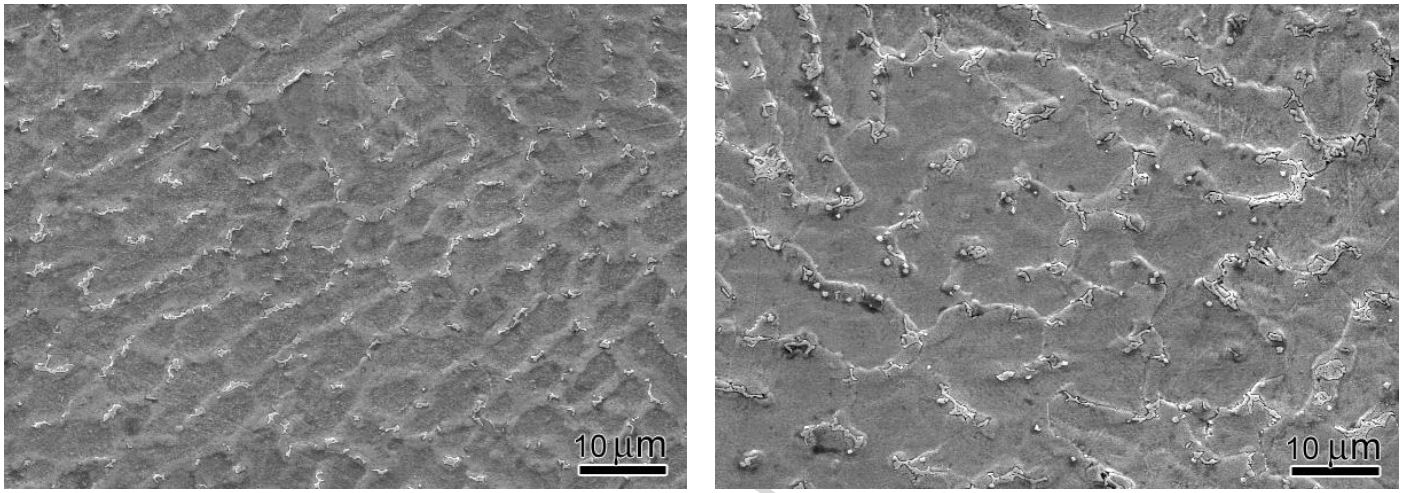

(a) (b)

Figure 6

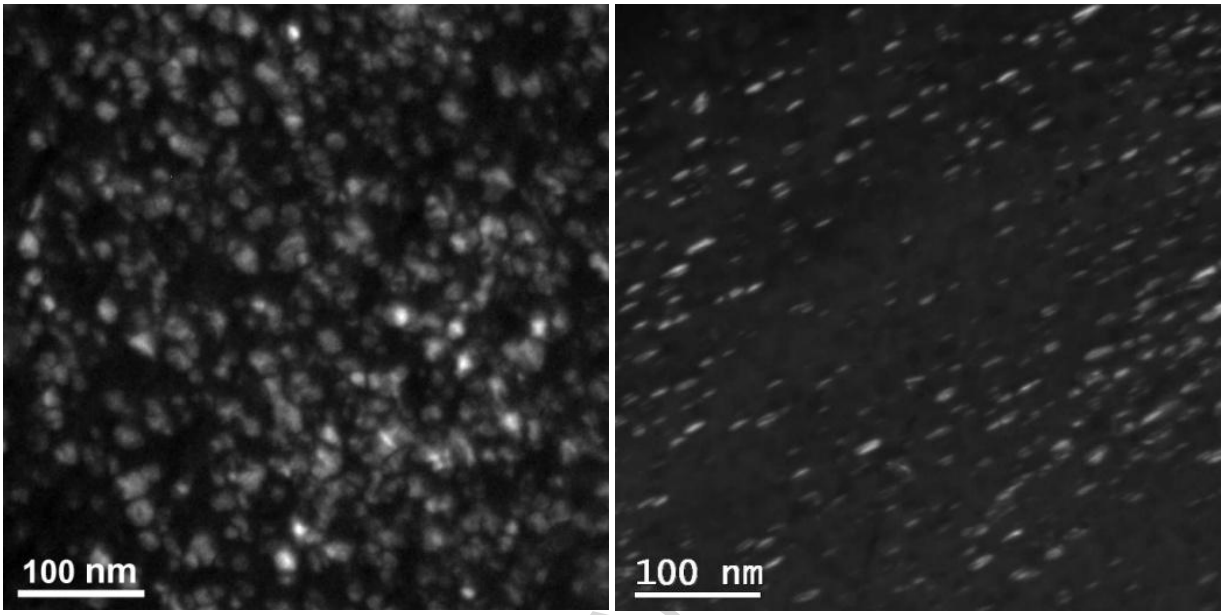

(a) (b)

Figure 7

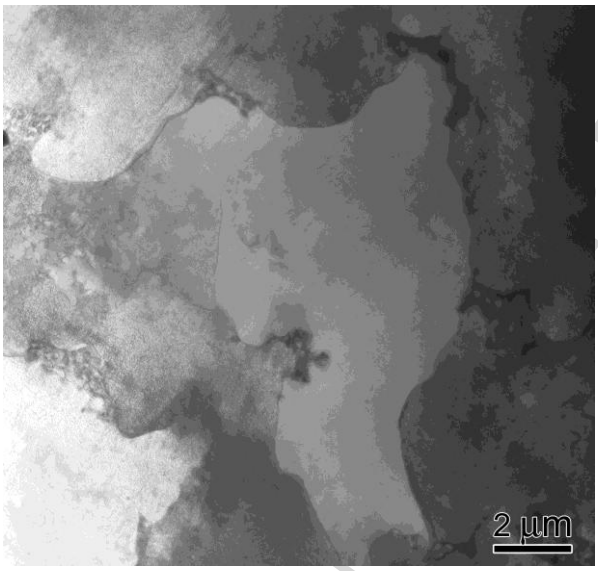

(a)

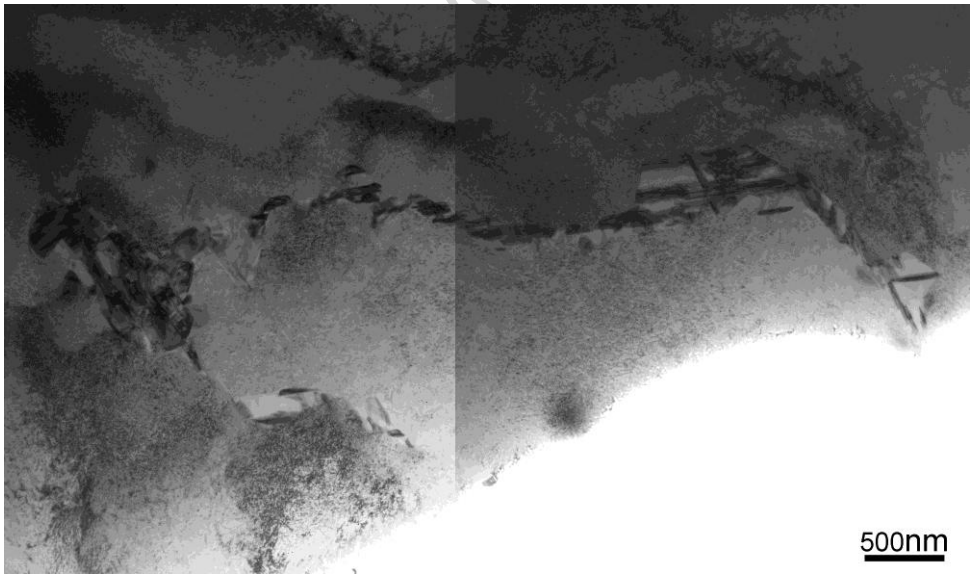

(b)

Figure 8

(a)

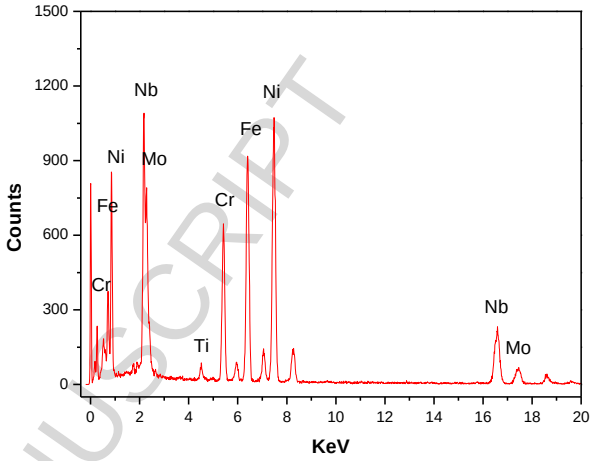

(b)

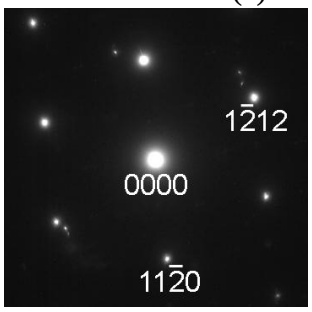

(c)

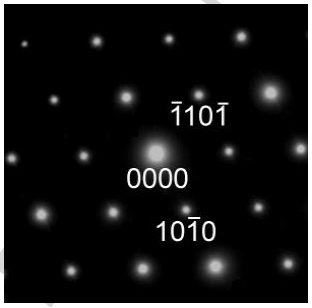

(d)

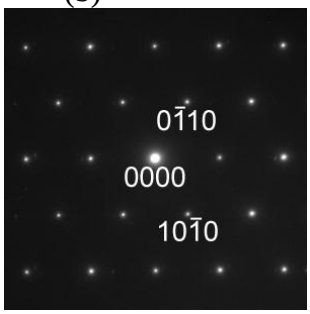

(e)

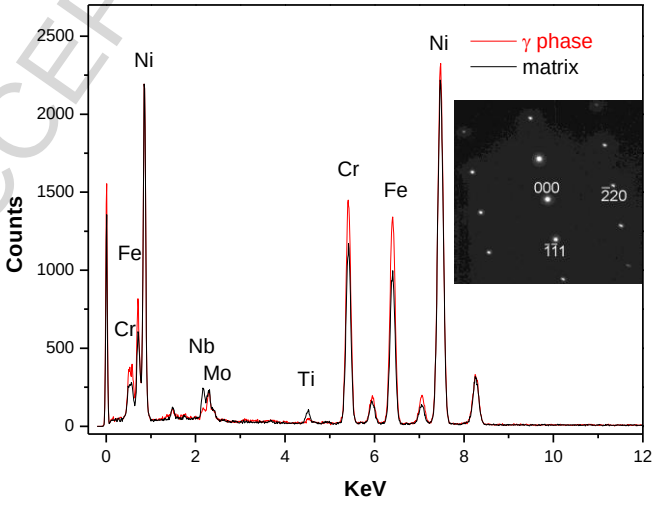

(f)

Figure 9

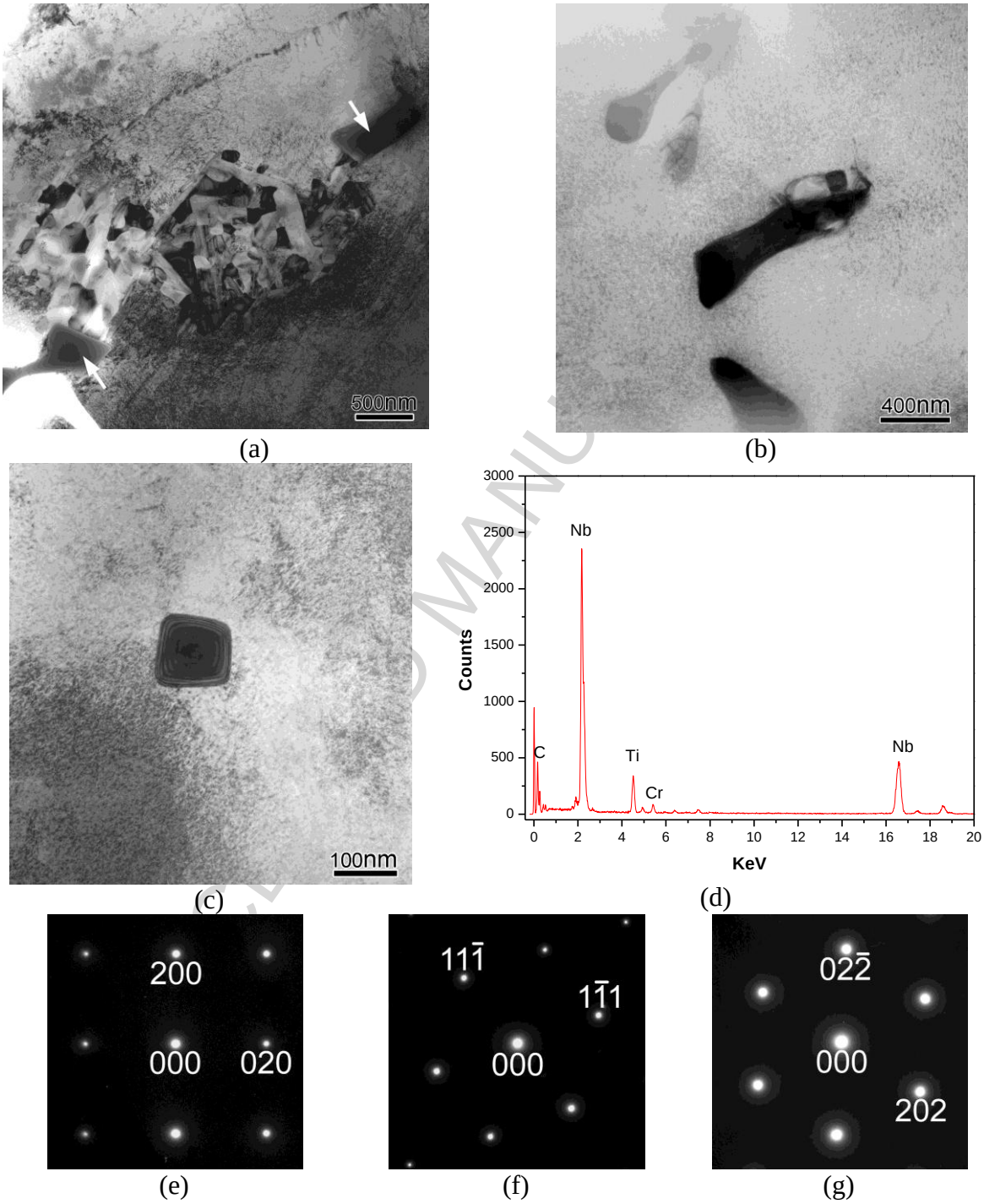

Figure 10

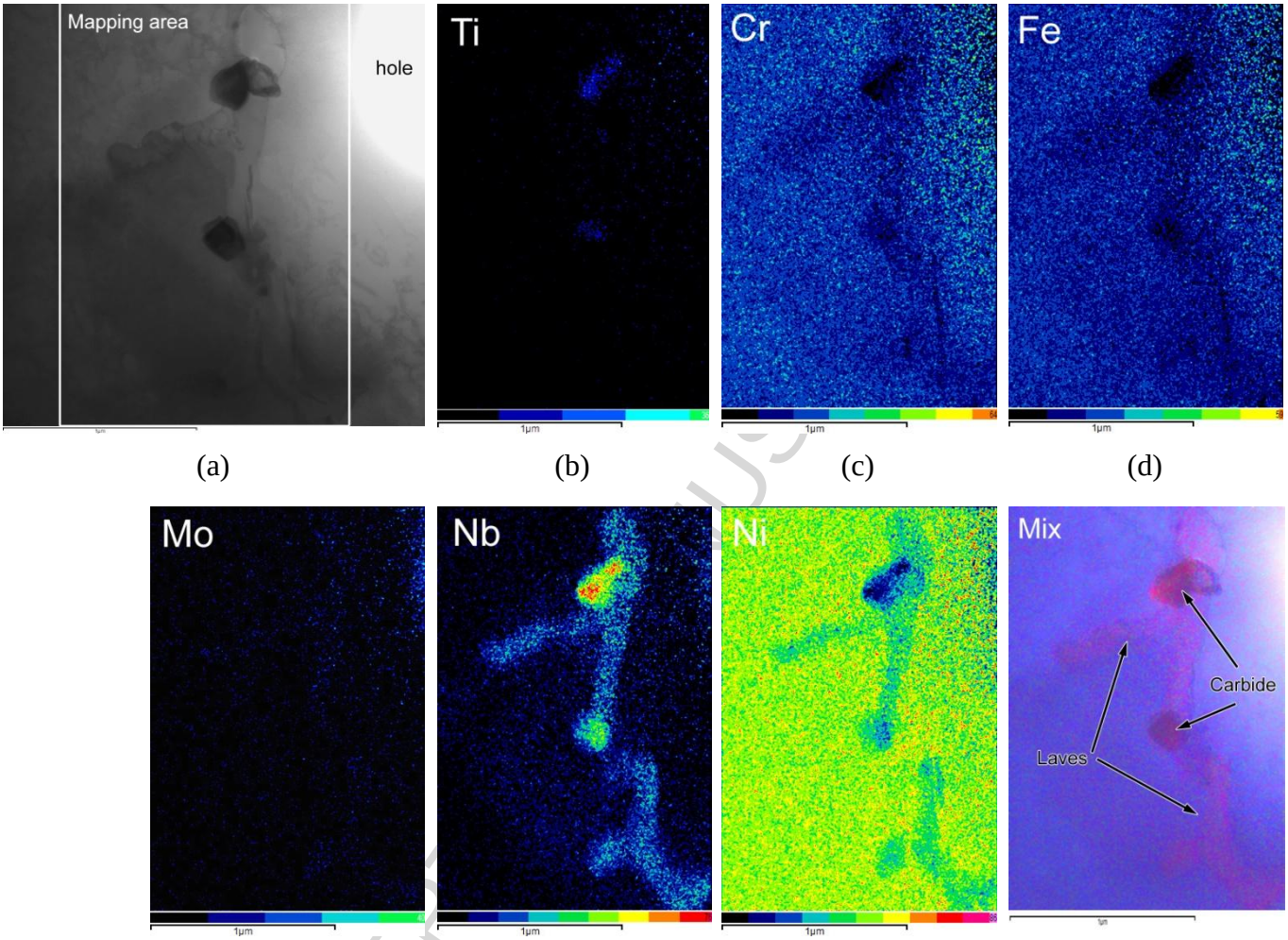

(a) (b) (c) (d)

(e) (f) (g) (h)

Figure 11

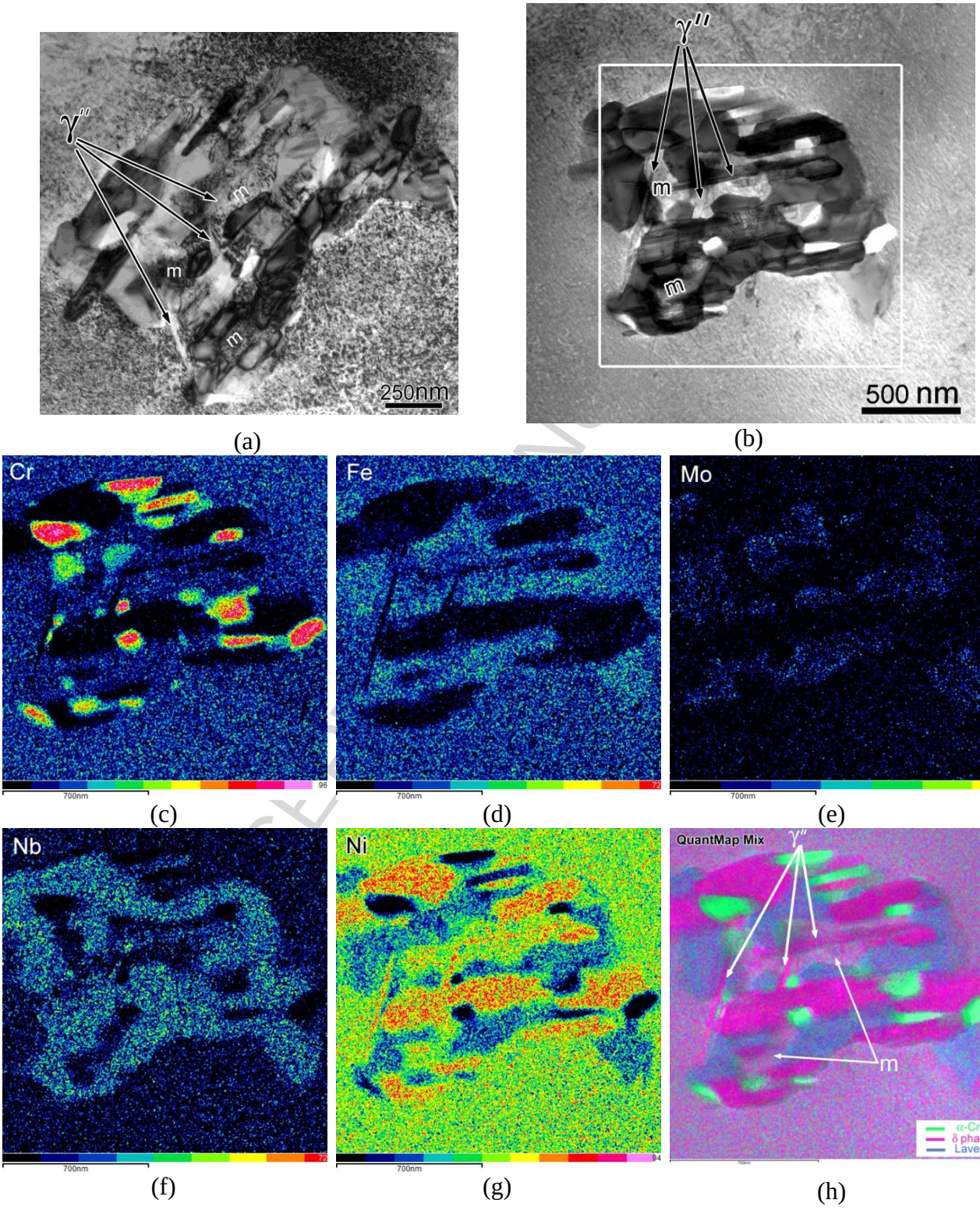

Figure 12

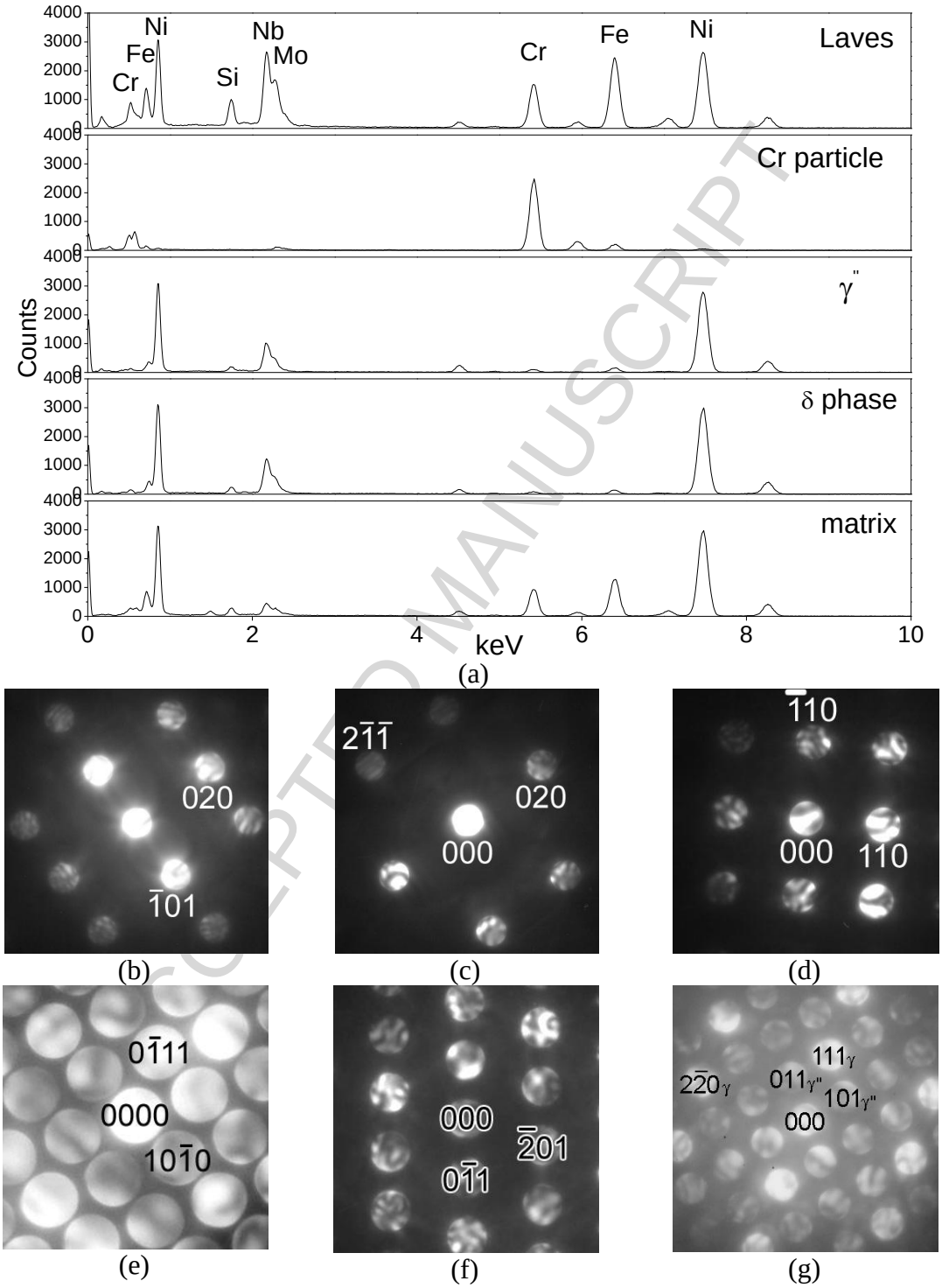

(a) (b) (c) (d) (e) (f) (g)

Figure 13

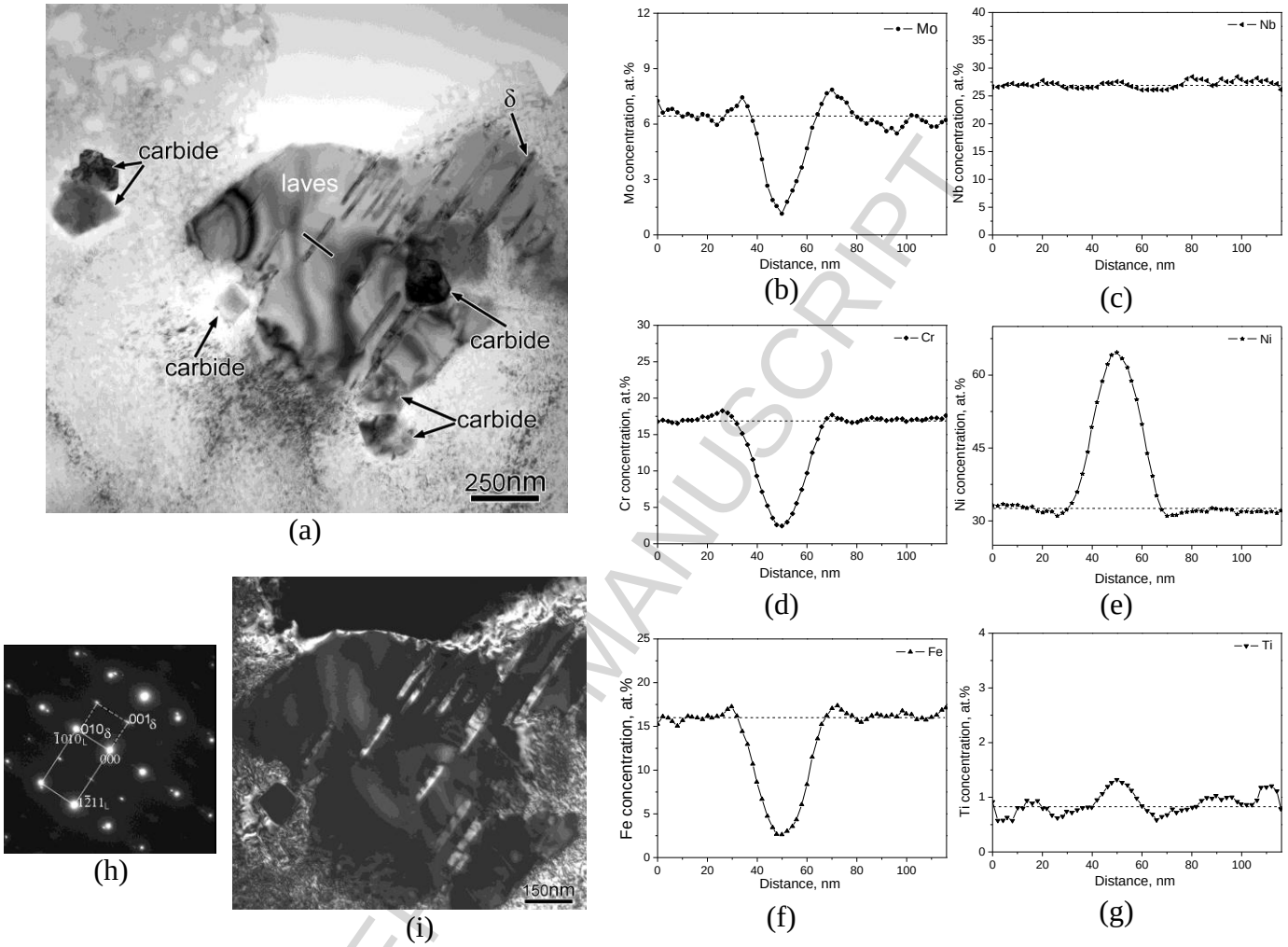

Figure 14

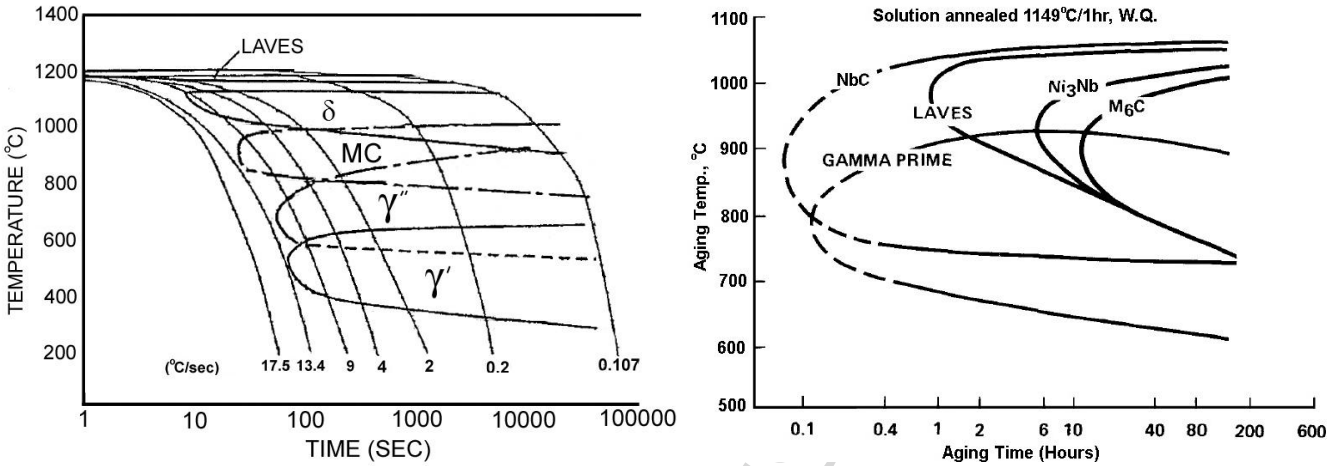

(a) (b)

Figure 15

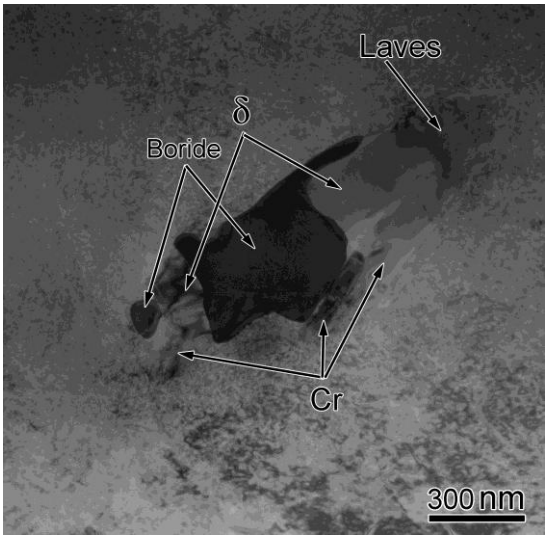

(a)

(b)

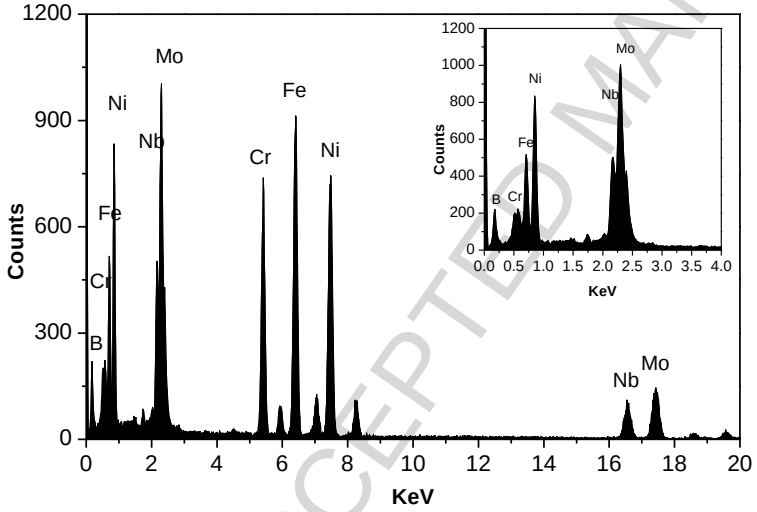

(c)

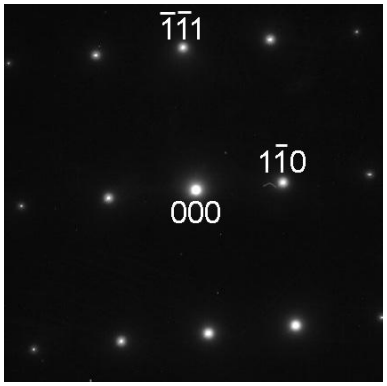

(d)

Figure 16

Figure Caption

Fig. 1 SEM (a) and TEM (b) images taken from the substrate show precipitates at grain boundaries and inside grains, and some twins (Fig. 1b); EDS spectrum taken from a precipitate shows that the composition is close to $(Ni,Cr,Fe)_3(Nb,Ti)$ (c); [100] (d); [011] (e) and [122] (f) diffraction patterns from the δ phase.

Fig. 2 The arrow shows linear features in the δ phase (a), high resolution image indicates that the linear feature is stack fault (b).

Fig. 3 Diffraction pattern (a) taken from the [001] zone axis shows the presence of γ′ and γ′′, dark field image (b) of γ′ obtained using the (110) reflection, and dark filed image (c) of γ′′ obtained using the $(1\frac{1}{2}0)$ reflection.

Fig. 4 Overview of the laser-fabricated blocks for sample A (a) and sample B (b).
Note: white dots are indents from hardness measurements.

Fig. 5 A montage SEM image (a) taken from the substrate and deposit of Sample A, showing fine grains in the substrate and coarse grains in the deposit, SEM image (b) taken from the substrate/deposit interface, showing a zone where the δ-phase was partially dissolved in the substrate.

Fig. 6 SEM images taken from transverse-sections of Sample A (a) and Sample B (b). Sample A has fine dendrite core and nearly continuous interdendritic regions and Sample B has coarse dendritic regions and semi-continuous interdendritic regions.

Fig. 7 Dark field images of γ′ obtained using the (110) reflection (a) and γ′′ obtained using the $(1\frac{1}{2}0)$ reflection (b).

Fig. 8 TEM images taken from the deposit of sample A show that particles may be distributed either discontinuously (a) or nearly continuously (b) at grain boundaries.

Fig. 9 TEM image (a) taken from the deposit of sample B shows γ/Laves eutectic, EDS spectrum (b) taken from the Laves phase in Fig. 8a shows that its composition is close to $(Ni,Cr,Fe)_2(Nb,Mo,Ti)$, $[\bar{2}203]$ (c), $[\bar{1}2\bar{1}3]$ (d) and [0001] (e) diffraction patterns from the Laves phase, EDS spectra (f) taken from the matrix and the γ phase, inset shows the [112] diffraction pattern from the γ phase.

Fig. 10 TEM images taken from the deposit of sample B show irregular carbides (a) (arrowed) and (b) and regular carbide (c), EDS spectrum from the carbide (d), [001] (e), [011] (f) and $[\bar{1}11]$ (g) diffraction patterns from the carbide.

Fig. 11 Bright field STEM image from sample A showing a mixture of carbides and Laves phases (a), EDS mapping for the marked area in Fig. 11a: Ti (b), Cr (c), Fe (d), Mo (e), Nb (f), Ni (g) and QuantMap Mix (h).

Fig. 12 Bright field TEM (a) and STEM (b) images from sample B show the morphology of a mixture of Cr-rich and Nb-rich phases, EDS mapping for the marked area in Fig. 11b: Cr (c), Fe (d), Mo (e), Nb (f), Ni (g) and QuantMap Mix (h).
Note: Fig. 12a and b were taken from the same area. Fig. 12 a (TEM image) clearly shows that there is matrix (marked by m) in the mixture.

Fig. 13 EDS spectra (a) of various phases in the mixture shown in Fig. 11, [101] (b), [102] (c), [001] (d) diffraction patterns from the Cr-particle, $[1\bar{2}1\bar{3}]$ diffraction pattern (e) from the Laves, [122] diffraction pattern (f) from the δ phase and $[11\bar{1}]$ diffraction pattern (g) from the γ′′.

Fig. 14 TEM image from sample A shows needle-like particles precipitated from the Laves phase (a), the concentration of Mo (b), Nb (c), Cr (d), Ni (e), Fe (f) and Ti (g) obtained by EDS linscan along the line in Fig. 13a, composite diffraction patterns from the Laves and the needle-like particle (h), dark field image of the needle-like particles (i).

Note: the dashed lines in the elemental profiles schematically present average contents of each element in the Laves phase.

Fig. 15 Continuous-Cooling-Transformation diagram of IN718 homogenised at 1180°C for 24 hours (a) [30], Time-temperature-transformation diagram of IN718 solution-annealed at 1149°C for 1 hour and water-quenched (b) [32].

Fig. 16 Borides connected to δ phases (a), borides nucleated on an MC carbide (b), a typical EDS spectrum from a boride (c), and [112] diffraction pattern of the boride (d).

	Element		Nb	Cr	Fe	Mo	Ti	Ni	Si	Al	Characteristic metal elements
Substrate	δ		23.0	2.0	3.0	1.0	3.0	67.0	0.5	0.5	
Deposit	MC carbide		85.0	1.0	/	/	14.0	/	/	/	δ: $(Ni,Cr,Fe)_3(Nb,Ti)$
	M_3B_2 boride		11.9	17.8	24.5	20.2	0.3	22.2	2.3	0.9	
	L+γ eutectic	L	25.0	15.0	20.0	8.0	1.5	30.0	0.5	/	
		γ	0.9	24.7	24.5	3.0	0.2	45	0.5	1.0	
	Complex constituent (e.g. Fig. 11)	Cr	/	87.0	8.0	2.8		2.0			Laves: $(Ni,Cr,Fe)_2(Nb,Mo,Ti)$
		L	21.6	12.5	20.7	5.6	1.6	30.0	7.6	0.4	
		δ	22.4	1.3	2.5	1.2	2.8	61.7	7.3	0.7	
		γ′′	20.2	1.9	3.0	1.0	4.8	62.7	6.2	0.2	
		m*	5.9	12.9	18.5	1.3	2.2	46.3	7.6	5.2	
	Needle-like δ in Laves	δ	26.0	1.5	2.0	1.0	1.0	67.0			
		L	26.0	17.0	16.0	7.0	0.5	33.0	0.5		

L - Laves

m* - γ+γ′+small γ′′

Table Caption

Table 1 List of typical phase compositions (at.%)

Highlights

- Secondary phases in IN718 deposits were identified using electron diffraction and EDS
- MC, M_3B_2, γ/Laves eutectic and γ/NbC/Laves eutectic were observed as in cast IN718
- Needle-like δ phase were precipitated from the Laves phase
- A complex constituent (Laves, δ, α-Cr, γ′ and γ) was reported for the first time